# Atmospheric controls and long range predictability of directional waves in the United Kingdom & Ireland

Timothy Scott[1], Gerhard Masselink[2], Robert Jak McCarroll[2], Bruno Castelle[3], guillaume dodet[4], Andrew Saulter[5], Adam A. Scaife[6], and Nick J. Dunstone[6]

[1]University of Plymouth
[2]Plymouth University
[3]CNRS, Université de Bordeaux
[4]IFREMER, Univ. Brest, CNRS, IRD, Laboratoire d'Oc eanographie Physique et Spatiale (LOPS), IUEM
[5]Met Office
[6]Met Office Hadley Centre

November 26, 2022

## Abstract

Improved understanding of how our coasts will evolve over a range of time scales (years-decades) is critical for effective and sustainable management of coastal infrastructure. Globally, sea-level rise will result in increased erosion, with more frequent and intense coastal flooding. Understanding of current and future coastal evolution requires robust knowledge of the wave climate. This includes spatial, directional and temporal variability, with recent research highlighting the importance of wave climate directionality on coastal morphological response, for example in UK, Australia and California. However, the variability of the inshore directional wave climate has received little attention, and an improved understanding could drive development of skillful seasonal or decadal forecasts of coastal response. We examine inshore wave climate at 63 locations throughout the United Kingdom and Ireland (1980–2017) and show that 73% are directionally bimodal. We find that winter-averaged expressions of six leading atmospheric indices are strongly correlated with both total and directional winter wave power (peak spectral wave direction) at all studied sites. Coastal classification through hierarchical cluster analysis and stepwise multi-linear regression of directional wave correlations with atmospheric indices defined four spatially coherent regions. We show that combinations of indices have significant skill in predicting directional wave climates (r= 0.45–0.8; p<0.05). We demonstrate for the first time the significant explanatory power of leading winter-averaged atmospheric indices for directional wave climates, and show that leading seasonal forecasts of the NAO skillfully predict wave climate in some regions.

1

1  **Atmospheric controls and long range predictability of directional waves in the United**
2  **Kingdom & Ireland**

3  **T. Scott[1], G. Masselink[1], R. J. McCarroll[1], B. Castelle[2], G. Dodet[3], A. Saulter[4], A. A.**
4  **Scaife[4,5] and N. Dunstone[4]**


5  [1] School of Biological and Marine Sciences, University of Plymouth, UK.

6  [2] University of Bordeaux/CNRS, UMR EPOC, Bordeaux, France.

7  [3] IFREMER, Univ. Brest, CNRS, IRD, Laboratoire d'Océanographie Physique et Spatiale,
8  IUEM, Brest, France.

9  [4] UK Met Office, Exeter, UK

10  [5] College of Engineering, Mathematics and Physical Sciences, University of Exeter, UK.

11  Corresponding author: Tim Scott

12  timothy.scott@plymouth.ac.uk

13  **Key Points:**

14  • Over 70% of inshore wave climates in United Kingdom and Ireland are directionally
15     bimodal

16  • Combinations of winter atmospheric circulation indices NAO, WEPA, SCAND and EA
17     are significantly correlated with directional wave climates in all regions

18  • Regression models using multiple winter atmospheric indices enable skillful
19     reconstructions of directional wave climate in all regions ($r^2 = 0.45$–$0.8$)

20  **Abstract**

21  Improved understanding of how our coasts will evolve over a range of time scales (years-decades) is
22  critical for effective and sustainable management of coastal infrastructure. Globally, sea-level rise will
23  result in increased erosion, with more frequent and intense coastal flooding. Understanding of current and
24  future coastal evolution requires robust knowledge of the wave climate. This includes spatial, directional
25  and temporal variability, with recent research highlighting the importance of wave climate directionality
26  on coastal morphological response, for example in UK, Australia and California. However, the variability
27  of the inshore directional wave climate has received little attention, and an improved understanding could
28  drive development of skillful seasonal or decadal forecasts of coastal response. We examine inshore wave
29  climate at 63 locations throughout the United Kingdom and Ireland (1980–2017) and show that 73% are
30  directionally bimodal. We find that winter-averaged expressions of six leading atmospheric indices are
31  strongly correlated with both total and directional winter wave power (peak spectral wave direction) at all
32  studied sites. Coastal classification through hierarchical cluster analysis and stepwise multi-linear
33  regression of directional wave correlations with atmospheric indices defined four spatially coherent
34  regions. We show that combinations of indices have significant skill in predicting directional wave
35  climates ($r^2 = 0.45$–$0.8$; $p<0.05$). We demonstrate for the first time the significant explanatory power of
36  leading winter-averaged atmospheric indices for directional wave climates, and show that leading
37  seasonal forecasts of the NAO skillfully predict wave climate in some regions.

38

## 1. Introduction

39

40    Sustainable coastal zone management requires a robust knowledge and understanding of
41    beach and coastal dynamics over time scales ranging from years to decades. While coastal
42    erosion is already a problem globally (Luijendijk et al., 2018; Mentaschi et al., 2018), climate
43    change will also affect the primary drivers of coastal change, driving sea-level rise (Cazenave et
44    al., 2014) and increased storminess in some regions of the world (Zappa et al., 2013, Scaife et al.,
45    2012). Globally, increased sea-level rise will result in increased erosion (Le Cozannet et al.,
46    2016), and increased frequency and intensity of coastal flooding along low-lying coasts (e.g.,
47    Vousdoukas et al., 2018). A key requirement for progressing our understanding of coastal
48    dynamics and shoreline evolution is a comprehensive knowledge of the forcing wave conditions,
49    including its variability in space and time. The relatively recent availability of multi-decadal
50    atmospheric sea-level pressure records (e.g., Poli et al., 2016; Antolínez et al., 2018), hindcast
51    directional wave timeseries (e.g., Dodet et al., 2010) and beach morphological records (e.g.,
52    Masselink et al., 2016a; Turner et al., 2016; Ludka et al., 2019) have provide new insights into
53    the importance of multi-decadal atmospheric variability in controlling inshore wave conditions
54    and beach dynamics.

55    Dodet et al. (2019) investigated decadal datasets of beach morphology along the Atlantic
56    coast of Europe and found that winter-averaged wave conditions play a key role in determining
57    shoreline response in regions that are dominated by cross-shore exchange (on-offshore) of beach
58    sediments on seasonal and greater timescales. Castelle et al. (2017) expanded on this and linked
59    the variability in winter wave conditions along the Atlantic coast of Europe to winter-averaged
60    atmospheric indices, notably the North Atlantic Oscillation (NAO; Hurrell, 1995) and the West
61    Europe Pressure Anomaly (WEPA). It was further demonstrated that the NAO was most strongly
62    correlated to the wave heights north of southern Ireland (52˚N) and that WEPA was most
63    strongly correlated to the wave heights from the south of Ireland to the south of Portugal. Dodet
64    et al. (2010) demonstrated for the first time the link between the winter averaged mean wave
65    direction variability and the winter-averaged NAO in the North East Atlantic, with positive
66    correlations up to 0.7 in South Portugal. Martínez-Asensio et al. (2016) also examined
67    relationships between the wind wave climate and the main climate modes of atmospheric
68    variability (1989–2007) in the North Atlantic Ocean (including NAO, East Atlantic (EA) pattern,
69    East Atlantic Western Russian (EA/WR) pattern and the Scandinavian (SCAND) pattern),
70    demonstrating that NAO and EA (which has similar characteristics to WEPA) patterns are the
71    most relevant. However, none of these studies have examined these relationships within
72    directionally multimodal wave climates, common to more sheltered and protected seas.

73    Along the exposed coasts of western Europe facing the dominant wave direction,
74    sediment movement and therefore beach response is mainly driven by cross-shore processes
75    (Castelle et al., 2014; Masselink et al., 2016a; Scott et al., 2016; Burvingt et al., 2018). In
76    contrast, beaches that are not directly facing the dominant wave approach, experience oblique
77    wave approach and longshore processes drive sediment transport and beach response (Short and
78    Masselink, 1999, Bühler and Jacobson 2001). Planform changes in beach orientation, which is
79    referred to as "rotation" and is typical of embayed settings (Klein et al., 2002), can be driven by
80    either spatial variability of cross-shore sediment transport, or longshore transport gradients.

81

82    Harley et al (2011) demonstrated that rotation can be linked to subtle variations in
83   alongshore gradients of wave energy, and hence cross-shore sediment exchange, leading to out-
84   of-phase response at embayment extremities. The most common rotation mechanism occurs in
85   relatively sheltered settings with a mixture of distant swell and local wind wave components
86   coming from different directions (i.e., bi-directional wave climate). In such environments, the
87   rotational response is governed by the relative importance of the two wave directions associated
88   with the bi-directional wave climate compared to the long-term average (Ruiz de Alegria-
89   Arzaburu and Masselink, 2010; Bergillos et al., 2016; Wiggins et al., 2019a). Year-to-year
90   changes in the directional variability in shoreline alignment in these settings are common, with
91   seasonal rotational phases often leading to erosion and increased coastal vulnerability at one or
92   other end of the embayment (e.g., Scott et al., 2016).

93    Recent (Pacific) basin-wide research into inter-annual wave climate variability in the
94   Pacific (Barnard et al., 2015; Mortlock and Goodwin, 2016) revealed links between climate
95   forcing (ENSO modes), wave direction and cross-shore beach response. Further to this,
96   modelling work by Splinter et al. (2012) and field observations by Harley et al. (2017) have
97   highlighted, not only the relationship between climate indices on wave direction and the
98   subsequent impact on shoreline dynamics along the east coast of Australia, but also the impact of
99   storm wave direction on coastal vulnerability along embayed coasts in general. In northwest
100  Europe, research by Wiggins et al. (2019a) shows that winter-averaged variability in NAO and
101  WEPA has significant skill in explaining wave directional balance in regions where wave
102  climate is strongly bi-directional, as well as driving beach rotation in these regions (Wiggins et
103  al., 2019b).

104   The NAO represents the principle mode of variability in the North Atlantic climate, and
105  the skillful predictability of winter NAO is critical for long-range forecasting of the European
106  surface winter climate (Wang et al., 2017). As an intrinsic mode of variability in atmospheric
107  circulation, the dynamics associated to the NAO have in the past been considered unpredictable
108  and largely stochastic in nature (Kim et al., 2012; Smith et al., 2016). But recent forecast systems
109  (Scaife et al., 2014; Dunstone et al., 2016) have shown significant skill provided large ensembles
110  are used (Athanasiadis et al 2016 report correlation skill of 0.86 with large multimodel
111  ensembles) due to the anomalously weak signal-to-noise ratio of climate signals (Scaife and
112  Smith, 2018), achieving correlation coefficients of $r > 0.6$ for winter season (DJF) forecasts
113  initiated on 1st November. Dunstone et al. (2016) highlighted potential for further improvements
114  in skill through increased ensemble size and decadal predictability of the NAO with large
115  ensembles was recently reported by Smith et al. (2019). Advances have also been achieved
116  through empirical approaches to forecasting the NAO. For example, Wang et al. (2017) used
117  multiple linear regression of key discriminant variables (sea-ice concentration, stratospheric
118  circulation and sea-surface temperature) and obtained forecast skill (r) of 0.69–0.71. Combined,
119  these advances suggest that skillful prediction of seasonal and decadal coastal vulnerability may
120  be possible (Colman et al 2011, Dobrynin et al., 2019), where forecasts of climate indices may
121  provide a valuable tool for managing risk to society due to extreme winter-wave events, wave
122  directional variability and corresponding geomorphological change at the coast.

123   An improved understanding of how leading atmospheric indices can explain seasonal to
124  multi-decadal variability in wave power and directionality, and consequentially beach state, lays
125  the foundation for: (1) new insights into climate controls on basin-scale coastal change; and (2)

126   potential exploitation of skillful season ahead and decadal forecasts of atmospheric indices. The
127   overall aim of this paper is to investigate whether climate variability, synthesized by leading
128   winter-averaged atmospheric indices (NAO, WEPA, EA, EA/WR, SCAND, and the Artic
129   Oscillation AO), significantly controls the directional balance of alongshore wave power at
130   inshore locations throughout the UK & Ireland (UK&I), characterized by directionally bimodal
131   (semi-) sheltered seas. The specific objectives are to: characterize the directional wave climate of
132   the UK & Ireland (Section 3); examine relationships between winter wave climate and leading
133   atmospheric indices (Section 4), exploring the regional coherence (Section 5); developing multi-
134   linear regression models for predicting winter directional wave climate (Section 5); and assessing
135   the current skill of season ahead forecasts to create useful predictions for coastal managers
136   (Section 6).

137   **2. Datasets**

138          2.1 Wave modelling

139          The directional wave climates throughout the UK&I were analyzed at 63 coastal
140   locations (~20m depth) using data from the UK Met Office 8-km WAVEWATCH III third-
141   generation spectral wave model (version 3.14; Tolman, 2009), representing a 3-hourly hindcast
142   of integrated wave parameters for the period 1980–2017. This model is described in detail by
143   Mitchell et al. (2017) and has been extensively validated with directional buoys and satellite
144   altimeters by Saulter (2015). These 63 sites were selected to represent all major stretches of
145   exposed coastline throughout the UK&I (Figure 1), and range from the extremely exposed storm-
146   dominated Atlantic west coasts of Ireland, Scotland and southwest England, to more sheltered
147   locally-derived wind-wave dominated regions in the Irish Sea, North Sea and English Channel.
148   Section 3 provides an overview of the annual wave climate in each region for 1980–2017.

149          Our analysis, including the use of peak spectral wave direction, relies on an assumption
150   that bimodality is primarily asynchronous. A preliminary analysis indicated that synchronous
151   bimodality, where the wave power of a secondary spectral peak is >5% that of the main peak,
152   occurs <5% of the total time. The lowest synchronous spectral bimodality occurred in semi-
153   sheltered coastal regions typically associated with bi-directional wave climates (S and E
154   England). Therefore, the assumption of asynchronous bimodality is justified, and references to
155   bimodality from herein refer to asynchronous bimodality.

156          2.2 Atmospheric data and climate indices

157          Climate indices used in this study include the leading monthly teleconnection indices
158   (NAO, EA, EA/WR and SCAND) derived from rotated EOF analysis of the monthly mean
159   standardized 500-mb height anomalies in the Northern Hemisphere, as described in Barnston and
160   Livezey (1987) and available for the period 1980–2017 (downloaded from the National Oceanic
161   and Atmospheric Administration (NOAA) Climate Prediction Center; www.cpc.ncep.noaa.gov).
162   In addition, we used the Western Europe Pressure Anomaly (WEPA), a climate index developed
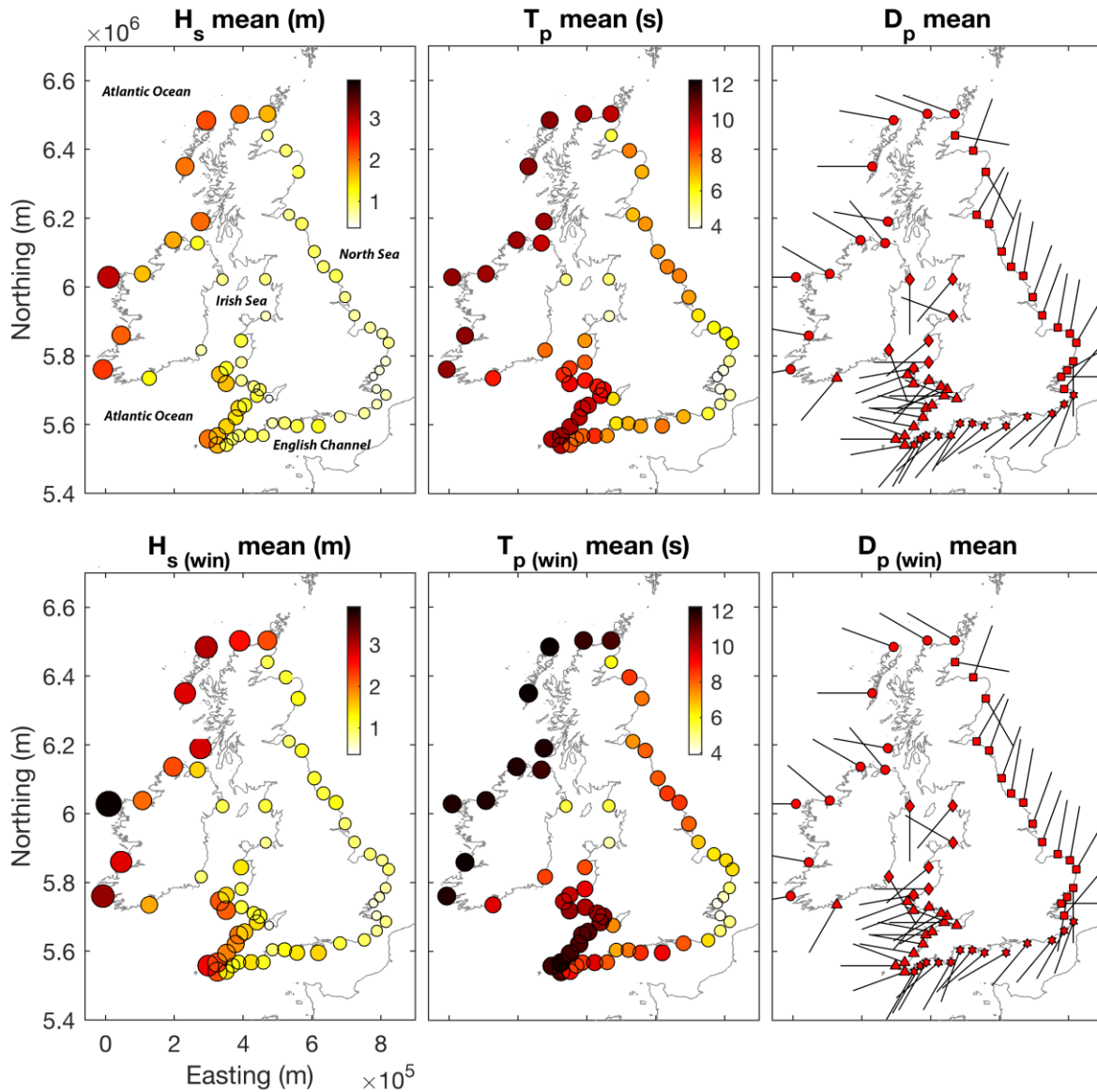163   by Castelle et al. (2017) and computed as the normalized sea level pressure (SLP) gradient

**Figure 1.** Overview of annual (top panels) and winter (bottom panels) wave climate (1980–2017) around the UK&I coast (all 63 wave model nodes) – mean significant wave height (left panels), mean peak wave period (middle panels), modal peak wave direction (frequency of occurrence; right panels). The size of symbols (left/middle) are proportional to colormap values.

164
165     between Valentia (Ireland) and Santa Cruz de Tenerife (Canary Islands). Although the WEPA
166     contains some variability of EOF-based NAO, EA, EA/WR and SCAND, it was used as it
167     provides a simple SLP-based index that best explains winter wave height variability along the
168     coast of western Europe, from UK to Portugal (52–36°N), and which reflects a latitudinal shift of
169     the Icelandic low / Azores high dipole. We also used the Artic Oscillation (AO), a climate index
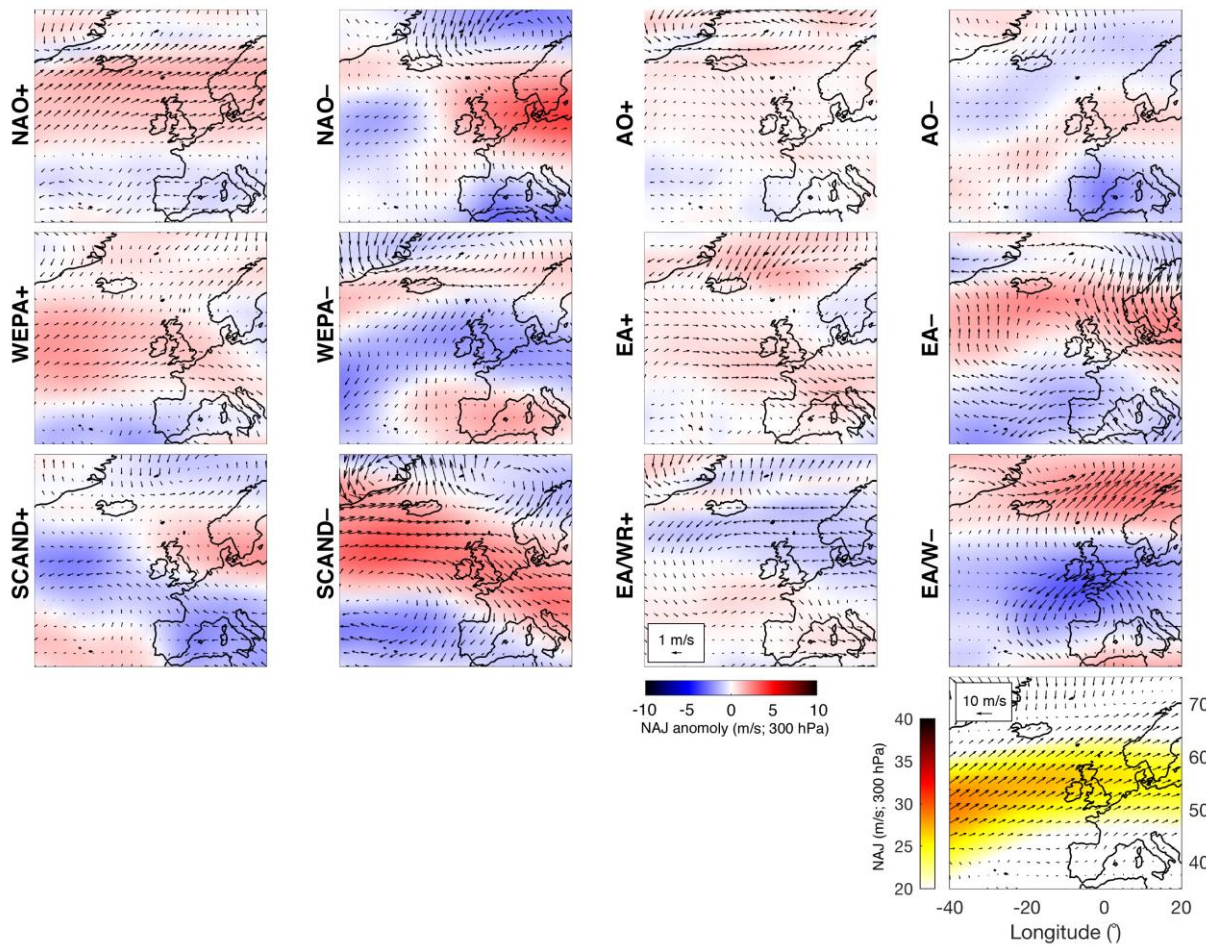
**Figure 2.** Atmospheric signature of all indices used in this study. Panels show sea surface wind (vectors) and 300 hPa winds relating to the North Atlantic Jet (NAJ; red/blue colours) anomalies from long term mean. Positive phase and negative phase of each index is addressed by averaging the 5 years with the largest and smallest index values over 1980–2017, respectively. Variability is displayed as anomalies from the long-term mean (1980–2017). Long-term mean sea surface wind field (vectors) and NAJ 300 hPa wind speed (colour) are shown in bottom right panel for entire period.

170
171   representing the state of the atmospheric circulation of the Arctic computed by projecting the AO
172   loading pattern to the daily 1000-mb height field anomaly above 20°N. The loading pattern of
173   the AO is the leading mode from EOF analysis of monthly mean 1000-mb height for 1979–2000.
174   While research has debated the usefulness of the AO, suggesting it is expressing the same
175   physical phenomenon as the NAO (Itoh, 2008), it is included in this study due to the potential
176   insights it may provide for subtle changes in directional wind-wave fields in sheltered seas.
177   These regional atmospheric signatures are highlighted in Figure 2, illustrating the association of
178   +NAO and -SCAND with increased westerly winds at high latitudes, and  -NAO and +SCAND
179   linked to reduction in westerly airflow and blocking of the North Atlantic Jet (NAJ). It is also
180   clear from Figure 2 that +WEPA represents a southward shift and strengthening of westerly sea
181   surface winds in North Atlantic.

182    Season-ahead retrospective forecasts (hindcasts) of the winter-averaged December-March
183 (DJFM) NAO and WEPA are provided by version 3 of the Decadal Prediction System
184 (DePreSys3) of the UK Met Office, as outlined in Dunstone et al. (2016). Forecasts were run for
185 winters over the period 1980–2016, with hindcasts initialized on 1st November each year. The
186 NAO is calculated using the Azores-Iceland definition (similar to that used in Dunstone et al.
187 (2016), but now for DJFM (December–March). There is a significant correlation skill score for
188 the season-ahead forecasts of the observed pressure-dipole based NAO r = 0.57 (p < 0.05).
189 WEPA is calculated using the Canaries-Ireland definition (similar to that used in Castelle et al.
190 2017) but there is poor correlation skill score for the season-ahead forecasts of observed
191 pressure-dipole based WEPA (r = 0.13, p >> 0.05).

192    Atmospheric data were derived from the National Centers for Environmental Prediction
193 (NCEP)/ National Center for Atmospheric Research (NCAR) Reanalysis 1 project (downloaded
194 from www.esrl.noaa.gov/psd/data/gridded/data.ncep.reanalysis.html), providing gridded (0.25˚ x
195 0.25˚) 4 times daily (0Z, 6Z, 12Z, and 18Z) vector winds at 17 pressure levels from 1948 to the
196 present (Kalnay et al., 1996).

197 **3. Wave climates in the UK and Ireland**

198    Figure 1 provides an overview of the 63 inshore wave data nodes that span all the
199 sheltered and exposed regions of the UK&I. These regions can be qualitatively separated into
200 their geographic regions based on their wave exposure (annual/winter mean wave climate) and
201 the characteristics of the directional modality of the wave climate (Table 1; Figure 3). Integrated
202 winter wave climate is composed of months December through to March (DJMF), following
203 previous analysis of climate indices (e.g., Castelle et al., 2017). To assess directional multi-
204 modality throughout the UK&I and investigate the explanatory power that climate indices may
205 have on the directional balance of alongshore wave power at these inshore locations, directional
206 modes were extracted from the cumulative directional wave power distribution for each wave
207 node around the coast and ordered by energy peak for 1980–2017 (Figure 3; right). Analysis of
208 direction modality shows that 46 of the nodes (73%) have directionally multimodal wave
209 climates where secondary modes (> 5% of primary mode peak prominence) have > 20˚ peak-to-
210 peak separation. Across all nodes, mean prominent peak half power width = 22˚; therefore, it can
211 be estimated that > 70% (~2.35$\sigma$) of peak distribution is within 20˚ of peak.

212    In general, the most exposed west coast regions (winter-averaged significant wave height
213 $H_s$ > 1.5 m and peak wave period $T_p$ > 9 s; W Ireland and SW England & Wales) display the
214 lowest levels of directional multimodality (20% and 33% of nodes, respectively) with NW
215 Scotland being the exception (60%) due to a broad ocean swell window (Table 1; Figure 1). All
216 nodes along the coasts of S & E England throughout the English Channel and North Sea coasts
217 are directionally multimodal; these regions are also the most sheltered from open ocean swell
218 and are the only regions where winter $H_s$ < 1.2 m. Moving up the North Sea coast into NE
219 Scotland, there is an increasing influence of northerly swell waves from the Arctic (winter $T_p$ =
220 7.4 s), but wave climate bi-directionality still dominates (100% of nodes) until the north-facing
221 coast of NW Scotland is reached. Coasts of W Wales, NW Wales & NW England, and E Ireland
222 are located within the Irish Sea with varying influence of S-SW Atlantic swell waves, resulting in
223 much of the region being dominated by local wind wave regimes and local influence of coastal
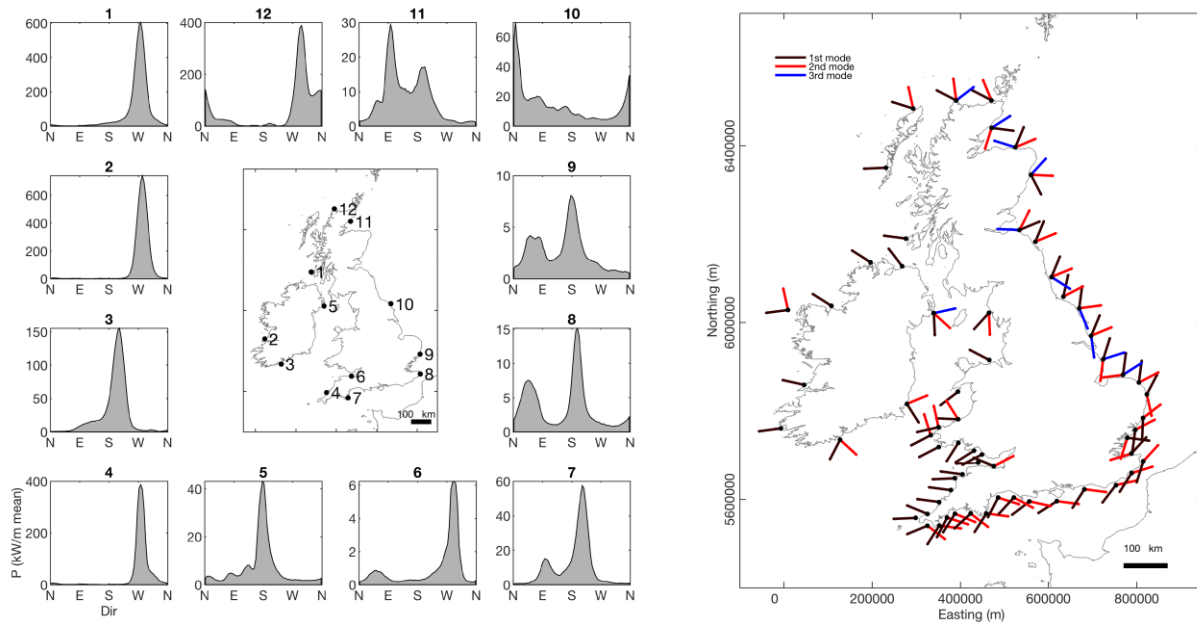224 orientation (winter $H_s$ = 0.9–1.3 m and $T_p$ = 5.1–9.4 s; Table 1).

**Figure 3.** Left: Regional examples of winter (DJFM) wave climate data showing distribution of directional wave power (cumulative). Insets are 3-hourly average kW/m in 5˚ bins for 1980–2017. Right: Quiver plot shows dominant directional modes (1980–2017) from cumulative wave power distribution for all coastal nodes. Black, red and blue are primary, secondary and tertiary, respectively. Modes displayed are > 5% of primary mode peak prominence.

**Table 1.** UK hindcast wave climate statistics for the period 1980-2016. Nodes shown in Figure 1 are integrated into regions of similar characteristics and exposure. Winter wave statistics represent months Dec-Mar.

| Region | Nodes(n) | Annual $H_s$ (m) | Annual $T_p$ (s) | Winter $H_s$ (m) | Winter $T_p$ (s) | Bi-directionality (%) |
|---|---|---|---|---|---|---|
| NW Scotland | 5 | 2.0 | 10.3 | 2.7 | 11.8 | 60 |
| W Ireland | 6 | 2.0 | 10.3 | 2.6 | 11.9 | 20 |
| SW England & Wales | 12 | 1.3 | 9.4 | 1.7 | 10.8 | 33 |
| W Wales | 4 | 1.2 | 8.2 | 1.5 | 9.4 | 75 |
| E Ireland | 4 | 1.0 | 7.9 | 1.3 | 8.7 | 75 |
| S England | 13 | 0.9 | 6.7 | 1.1 | 7.5 | 100 |
| NE Scotland | 3 | 0.9 | 6.7 | 1.1 | 7.4 | 100 |
| NW Wales & NW England | 2 | 0.7 | 4.8 | 0.9 | 5.1 | 50 |
| E England | 14 | 0.7 | 6.1 | 0.9 | 6.6 | 100 |

226    Initial wave climate analysis indicates that beyond the semi-sheltered sites examined in Wiggins
227    et al. (2019) along the western English Channel coast, directionally bimodal wave climates exist
228    in many inshore regions throughout the coasts of the UK&I. Of particular interest are nodes
229    along the English Channel coast (S England) and southern North Sea coast (E England) where
230    primary and secondary directional modes are from opposing directions with respect to the coastal
231    shore-normal, therefore having the greatest potential to influence coastal morphodynamics and
232    shoreline plan-shape rotation with respect to the directional balance of alongshore wave power
233    (Figure 3).

234    **4. Role of atmospheric indices**

235          The associations between long-term atmospheric forcing and wave climate, for inshore
236    waters of UK&I, were investigated by correlating the winter-averaged climate indices (NAO,
237    WEPA, SCAND, AO, EA and WR/EA) with total winter-averaged wave power (1980-2017), for
238    nodes in Figure 4. All references herein to climate indices are DJFM winter averaged. Total
239    winter-averaged wave power was found to be significantly correlated with NAO for Atlantic NW
240    coasts ($r = 0.6$–$0.83$; $p < 0.05$), consistent with earlier findings (Martínez-Asensio et al., 2016;
241    Castelle et al., 2017). Correlations for the Atlantic SW and within the Irish Sea were also
242    significant, though with lower coefficients ($r = 0.39$–$0.58$; Figure 4). Similar spatial relationships
243    occur for the AO, though limited to the west Atlantic, and with lower coefficients ($r = 0.5$–$0.8$,
244    Atlantic NW; $r = 0.31$–$0.4$, Atlantic SW). As previously determined (Castelle et al., 2017), the
245    NAO has limited skill in predicting total wave power south of southern Ireland (~52˚N), with
246    WEPA and EA displaying a corresponding increase in skill in this region. WEPA and EA only
247    show positive correlations with wave power for the southern half of UK&I, with WEPA
248    outperforming EA (15% greater explanation of variance, where significant correlations exist).
249    WEPA has the greatest predictive skill in the southwest ($r = 0.66$-$0.79$, Atlantic SW coast; $r = $
250    $0.81$-$0.84$, W English Channel). Wave power along the Atlantic NW exposed coast are also
251    correlated with negative SCAND ($r = -0.32$ to $-0.63$), while the semi-sheltered North Scotland
252    coast is correlated with positive SCAND ($r = 0.21$–$0.6$). The significance map of SCAND is
253    broadly an inverse of the AO.

254          In the context of previous ocean basin-scale research, significant positive relationships
255    with the NAO, AO, WEPA and EA, and also negative SCAND, for total wave power on Atlantic
256    coasts were expected, but inshore regional scale (including shelter seas) analysis here reveals
257    significant negative correlations with NAO/AO and positive correlations with SCAND along the
258    mixed swell/wind-wave dominated east-facing North Sea coast (NAO $r = -0.28$ – $-0.69$; AO $r = $ -
259    $0.41$ – $-0.71$, SCAND $r = 0.33$ – $0.65$) with AO showing the strongest relationship and level of
260    significance (all sites significantly correlated at 95% level). This analysis shows that the EA/WR
261    index provides the least explanatory power of all the indices tested.

262          The associations between wave direction and climate were further explored by
263    correlating the climate indices with cumulative directional winter wave power, within an angular
264    window spanning ±20° of the modal peak (Figure 5). Results show a striking degree of
265    correlation across multiple indices (NAO, AO, WEPA, EA, SCAND), with strong contrasts
266    between indices. This indicates that a significant amount of winter-wave directional variability
267    within UK&I can be explained by variations in climatic modes, with correlations apparent even
268    for some sheltered wind-wave dominated regions away from Atlantic swell.
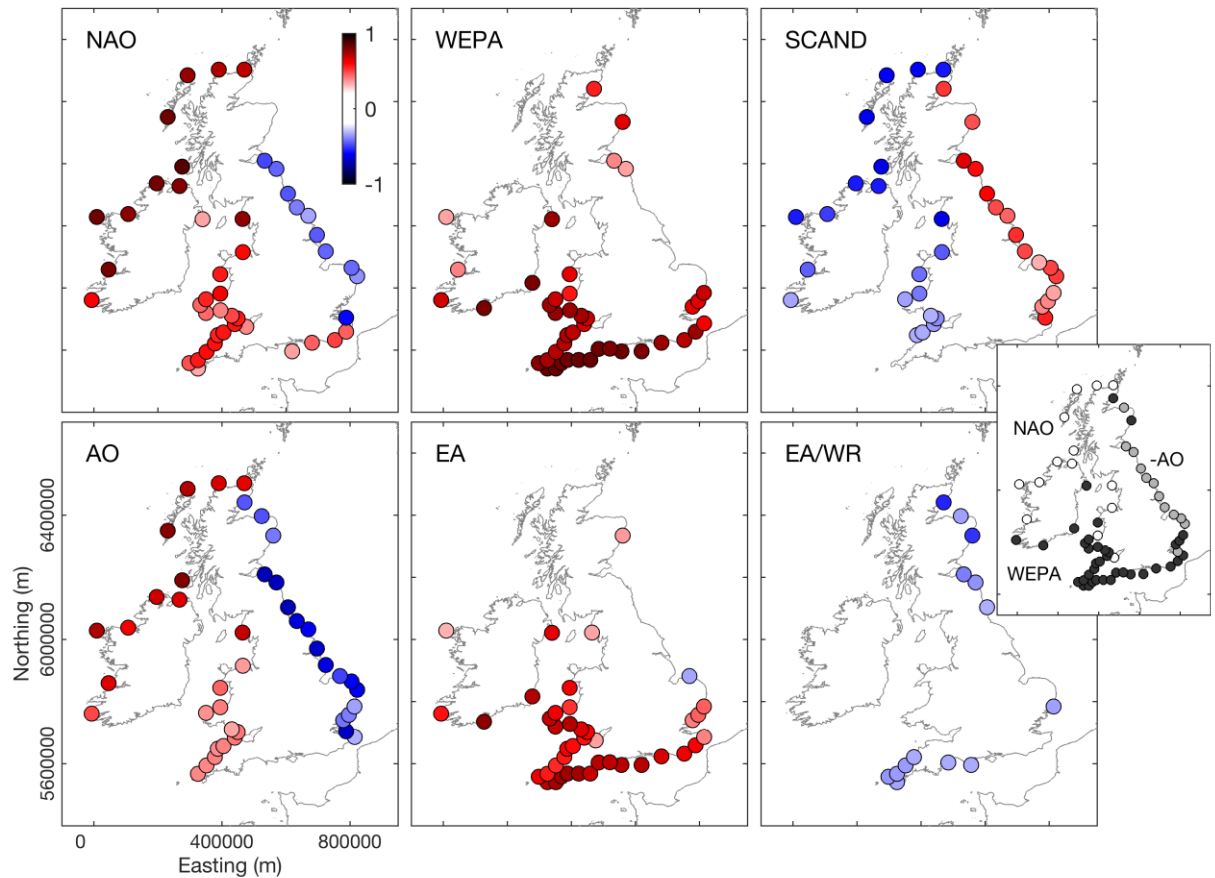
**Figure 4.** Correlations between mean winter wave power and six winter-averaged atmospheric indices (NAO, WEPA, SCAND, AO, EA and EA/WR) for 63 locations around the coast of the UK&I. Only locations where correlation coefficients (r) were significant at 95% level are shown (p<0.05). Inset shows leading explanatory index for each node (white = NAO, black = WEPA, grey = AO).

269
270

271        All nodes in the southern Ireland, English Channel and southern North Sea coasts (south-
272    facing) are strongly directionally bimodal (Figure 3), with coastal orientation suggesting
273    dominance of alongshore sediment transport processes, which is supported by observations along
274    this coast by Wiggins et al. (2019b). Analysis shows that WEPA (and EA to a lesser extent)
275    significantly explains variability in winter-averaged wave power for all southwesterly orientated
276    (principal) wave directional modes (r = 0.58–0.77), accounting for the largest proportion of
277    winter-averaged wave power. In contrast, negative NAO explains variability in all easterly-
278    orientated wave modes (r = -0.6 – -0.76), with positive SCAND also contributing high
279    correlations with easterly waves (r = -0.5 – -0.67). These findings mean the full winter-averaged
280    directional wave power balance is significantly explained by climate indices along this whole
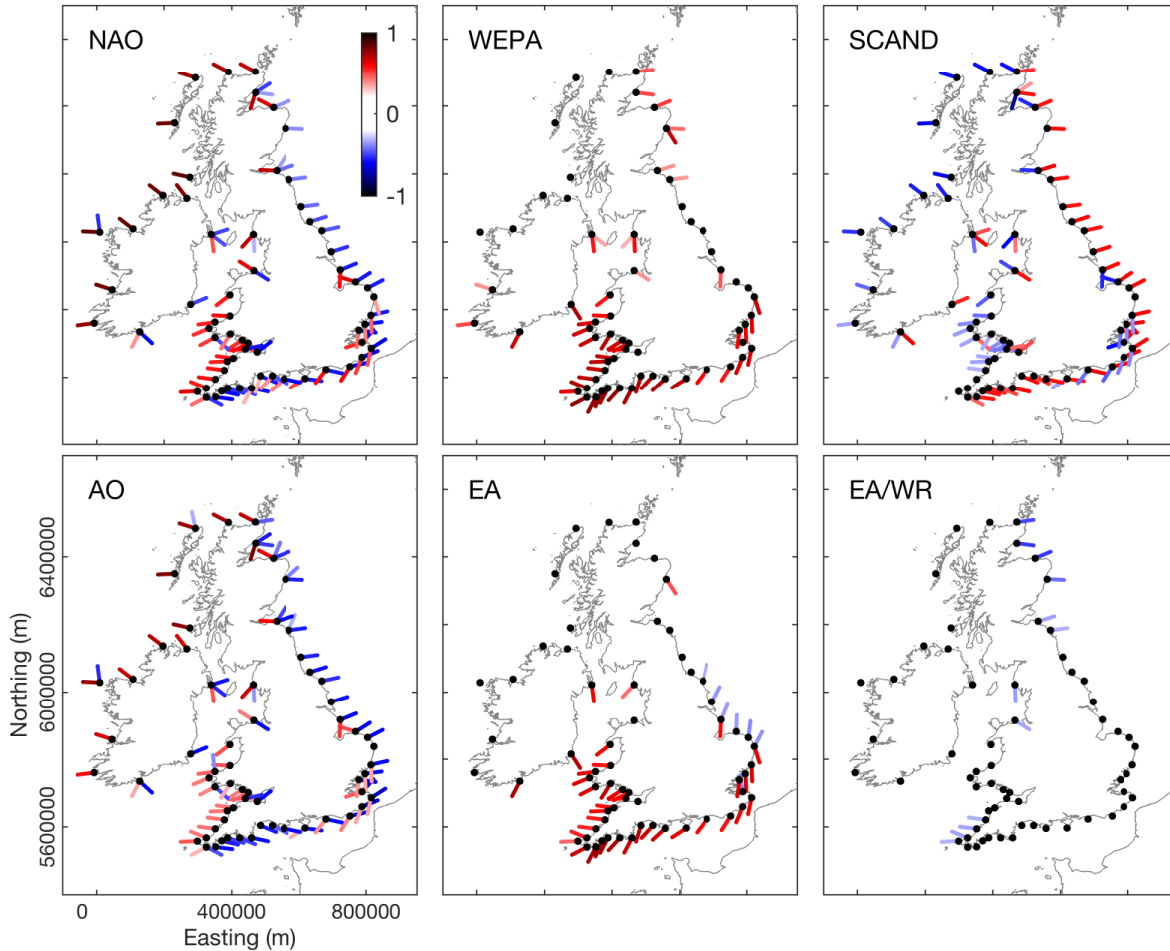281    section of coast.

**Figure 5.** Relationship between winter-averaged NAO, WEPA, SCAND, AO, EA and EA/WR and directional winter-averaged wave power (local wave directional window of +/- 20˚ for each node) for 63 wave nodes (black dots) around the coast of the UK&I (1980–2017). Colors are correlation coefficients (r), only results where P < 0.05 are shown.

282
283 Beyond the south coast regions, easterly-orientated wave modes throughout the bi-directional
284 North Sea region, characterized by short wind-waves, showed significant relationships with
285 negative NAO (and AO) where r = -0.35 – -0.57 (r = -0.5 – -0. 62) decreasing to the north. The
286 strongest relationships in the North Sea region are found with the SCAND index, showing
287 significant positive correlations with all easterly-orientated nodes where r = 0.57–0.62.
288 Interestingly, EA and AO, and NAO to a lesser extent, had some skill in explaining northerly
289 swell waves entering this North Sea region, but only regionally. This northerly component is an
290 important element of the northern North Sea coastal wave climate and is associated with a small
291 swell window and is strongly impacted by coastal orientation. Whilst EA provided some skill in
292 explaining northerly wave mode variability at six southern North Sea coast sites, significant r-
293 values only reached 0.39. AO and NAO showed some explanatory power for six nodes in the
294 northern North Sea regions (E. Scotland) with significant r-values between 0.33 and 0.59 (Figure
295 5).

296     Throughout the UK&I there are sheltered regions with complex coastal orientations (e.g.,
297   E Scotland, Irish Sea and Bristol Channel) sheltered from significant swell-wave contribution
298   and that are dominated by a locally generated wind-wave climate. The directional wave modes in
299   these regions display a variety of significant relationships with indices dependent of spatial
300   location and coastal orientation. Typically, easterly-oriented short fetch nodes are related to
301   negative NAO/AO, and positive SCAND; whereas westerly-oriented short fetch nodes are
302   related to positive NAO/AO, and negative SCAND.

303     In summary, winter-averaged climate indices show strong and significant correlations
304   with directional winter-averaged wave power throughout the UK&I. Analysis indicates there are
305   regionally-coherent relationships between directional waves and various combinations of the
306   leading climate indices. To examine the temporal variability and predictability of regional
307   response characteristics, a quantitative connectivity-based cluster analysis is first undertaken.

## 5. Characterization of regional response

309     Regionally-coherent relationships between the climate indices shown to provide the most
310   explanatory power in determining directional wave variability in UK&I were investigated
311   through hierarchical cluster analysis. For all 63 nodes, the variables examined were mean
312   directional winter wave power correlation coefficients with NAO, WEPA, AO, SCAND and EA
313   for the period 1980–2017. EA/WR was excluded at this stage as spatial correlations were weak
314   and mostly statistically insignificant. EA and AO were retained as they provided some
315   explanatory skill for northerly waves in the North Sea. The clustering uses Euclidian-based
316   proximity to determine similarity between nodes where response variables are primary and
317   potentially secondary directional mode correlations with winter-averaged climate indices. The
318   dendrogram shown in Figure 6 shows the results of the cluster analysis where Ward's minimum
319   variance method is used to minimizes the total within-cluster variance (weighted squared
320   distance between cluster centers) at each step (Ward 1963). The advantage of Ward's method is
321   that it often provides a clear threshold number of groups where there is a large jump in group
322   merging cost (e.g., above and below similarity level 1; Figure 6).

323     Four clear groupings were defined by this classification process (Figure 6). Two groups
324   named South West and North West clearly represent the largely directionally uni-modal west
325   coasts that are dominated by ocean swell waves. A group named South represents nodes that are
326   bi-directional in nature and largely located on the southern and western regions of the UK&I.
327   The final major group named East also represents bi-directional wave climates, but the region is
328   limited to the eastern North Sea coast and only consists of sites exposed to northerly swell
329   waves. To elucidate the driving climate control relationships of each group, example nodes (A-E;
330   Figure 6) representing case study sites from each cluster, were examined further.

331     Figure 7 examines the atmospheric indices controlling the wave climate at each case
332   study site. Where the wave climate is directionally uni-modal, the standardized long-term (1980–
333   2017) winter-mean wave power timeseries is examined through a wave power index ($P_{index}$).
334   Where the wave climate is significantly directionally bimodal, a wave power directionality index
335   (WDI) is computed following Wiggins et al. (2019a), which represents the winter-averaged
336   standardized wave power balance between two opposing wave directional modes, shown by
337   Wiggins et al. (2019b) to correlate with observed beach rotation. At each node, an index of the

338    relative balance between winter wave power contributions from the two modal directions is
339    computed, using the equation:

$$WDI = \frac{(P_1 - P_2) - \overline{(P_1 - P_2)}}{\sigma(P_1 - P_2)} \tag{1}$$

340
341    where $(P_1 - P_2)$ is the residual wave power between the first (prominent) and second directional
342    wave power modes, $\overline{(P_1 - P_2)}$ is the long-term mean and $\sigma(P_1 - P_2)$ is the long-term standard
343    deviation of that difference. High positive values of WDI indicate that the primary directional
344    mode is more prevalent than the long-term average, whereas high negative values indicate that
345    the wave climate has a higher proportion of the secondary directional mode than average.
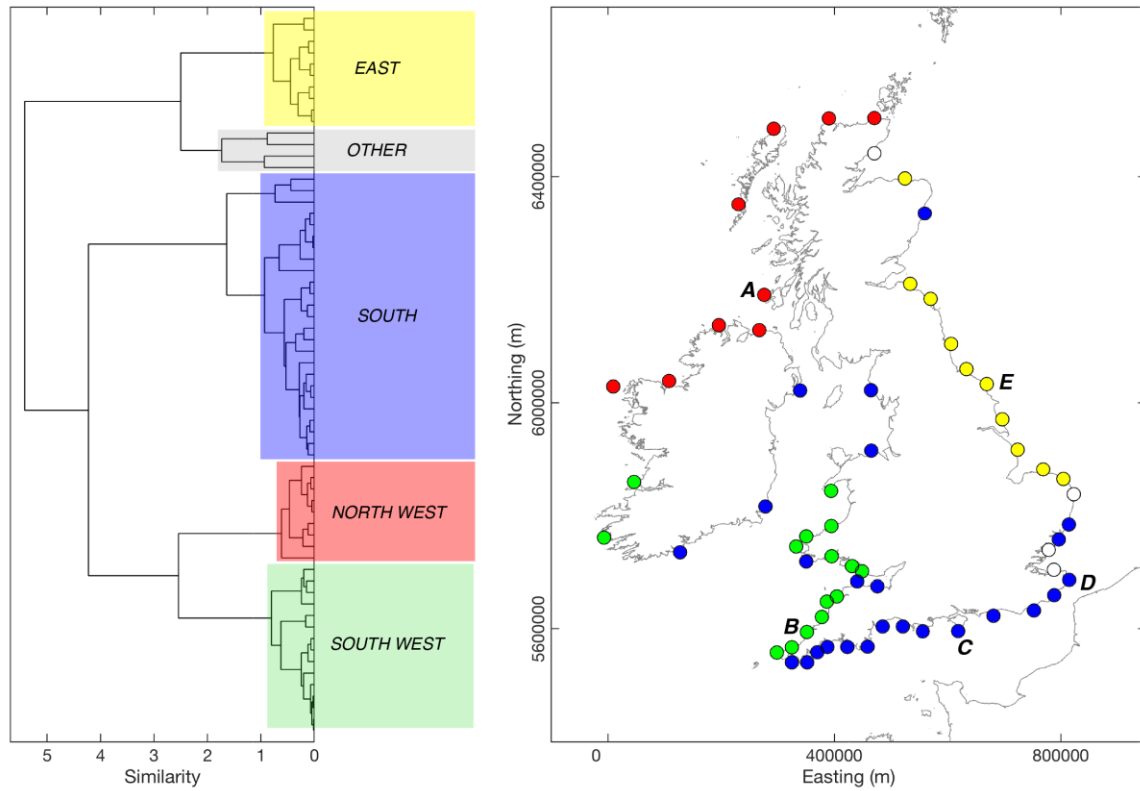


**Figure 6.** Regional classification of correlations between winter-averaged directional wave climate response (mean wave power for dominant directional modes) and most significant winter-average atmospheric indices NAO (EOF-based), WEPA (station-based), and SCAND (EOF-based) for the period 1980–2017. Left: Dendrogram illustrating results of hierarchical agglomerative cluster analysis, using Ward's minimal increase of sum-of-squares Euclidian proximity method. Clear groupings are labelled. Right: Groupings from cluster analysis presented spatially, with nodes A-E representing case-study sites from each region used for further analysis and visualization.

346

347    For all bi-directional example sites shown in Figure 7, WDI time-series show significant
348    temporal variability over the 37-year period. WDI within the South region (sites C and D; Figure
349    7 left panel) displays a consistent 5–8 year cyclicity that can be observed from the continuous
350    wavelet transform analysis shown in Figure 7 (right panels) computed as in Castelle et al. (2018)
351    using a scaled and normalized Morlet function, following Grinsted et al. (2004). Periodicity is
352    strongest and most significant since 2005. This corresponds to the periodicity observed in the
353    WEPA index by Castelle et al. (2018) through similar wavelet analysis. WDI at these South
354    group sites is significantly positively correlated with WEPA, NAO and SCAND, with WEPA
355    having a stronger correlation in the west of the region (site C) and NAO/SCAND increasing in
356    importance the east (site D). The case study site from the East group in the mid North Sea coast
357    (site E) shows a significant 5–6 year periodicity in WDI, but with limited negative phases
358    between 2000–2010 and shows weak or insignificant correlations to the climatic indices tested,
359    with the exception of SCAND. As has already been shown, example sites from North West and
360    South West groups, which are directionally uni-modal, $P_{index}$ are strongly correlated with NAO
361    and WEPA, respectively, and are therefore dominated by any periodicity of these indices. Unlike
362    WEPA, there is little coherent periodicity displayed within NAO dominated sites (site A) and
363    there are high degrees of variability over the period 1980–2017, with the only significant
364    timescales of ~2 years occurring post 2010 (Figure 7a-b; right panel). This lack of NAO
365    periodicity has previously been demonstrated by Barbosa et al. (2006) and Castelle et al. (2018).

366    It is clear that the inter-annual variability of winter-averaged directional wave power
367    throughout the UK&I is well explained by a range of individual indices, but it is useful to
368    explore whether or not when combined they have greater predictive skill, particularly for bi-
369    directional regions. Empirical stepwise multiple linear regression models were computed for
370    each example site using combinations of the leading indices for each location based on
371    correlation analysis and their predictive skill is presented in Figure 7 (left panels). For all sites,
372    except site A in the North West group, the combination of multiple indices in a linear model
373    outperformed the use of a single index. The model elements are presented in Table 2. Both sites
374    from exposed uni-directional groups (North West and South West) demonstrated very skillful
375    reconstructions of winter wave power with combinations of NAO and WEPA with r-squared
376    values exceeding 0.75. Specifically, site B from the South West group demonstrated the
377    improved skill gained by utilizing the product of two indices (r-squared = 0.8). WDI from the
378    South group (sites C and D) was skillfully predicted utilizing a combination of NAO, WEPA and
379    SCAND. The discriminatory power of these combined indices is visualized in NAO/WEPA and
380    NAO/SCAND parameter space (Figure 7; middle panels) demonstrating, for example, that at site
381    C all winters experiencing positive WDI occurred when both NAO and WEPA were positive.
382    Likewise, SCAND when combined with EA at site D accounts for a greater proportion of the
383    variance in WDI. Finally, in the East region (site E), where SCAND was the only index
384    significantly correlated with WDI (r = 0.35), the combination of NAO, WEPA and SCAND with
385    EA generated a linear model with significant explanatory skill (r-squared = 0.45), where the
386    combination of SCAND and EA at site D go some way in discriminating between WDI+
387    (dominance of waves from the northerly mode; EA–) and WDI– (waves from the easterly mode;
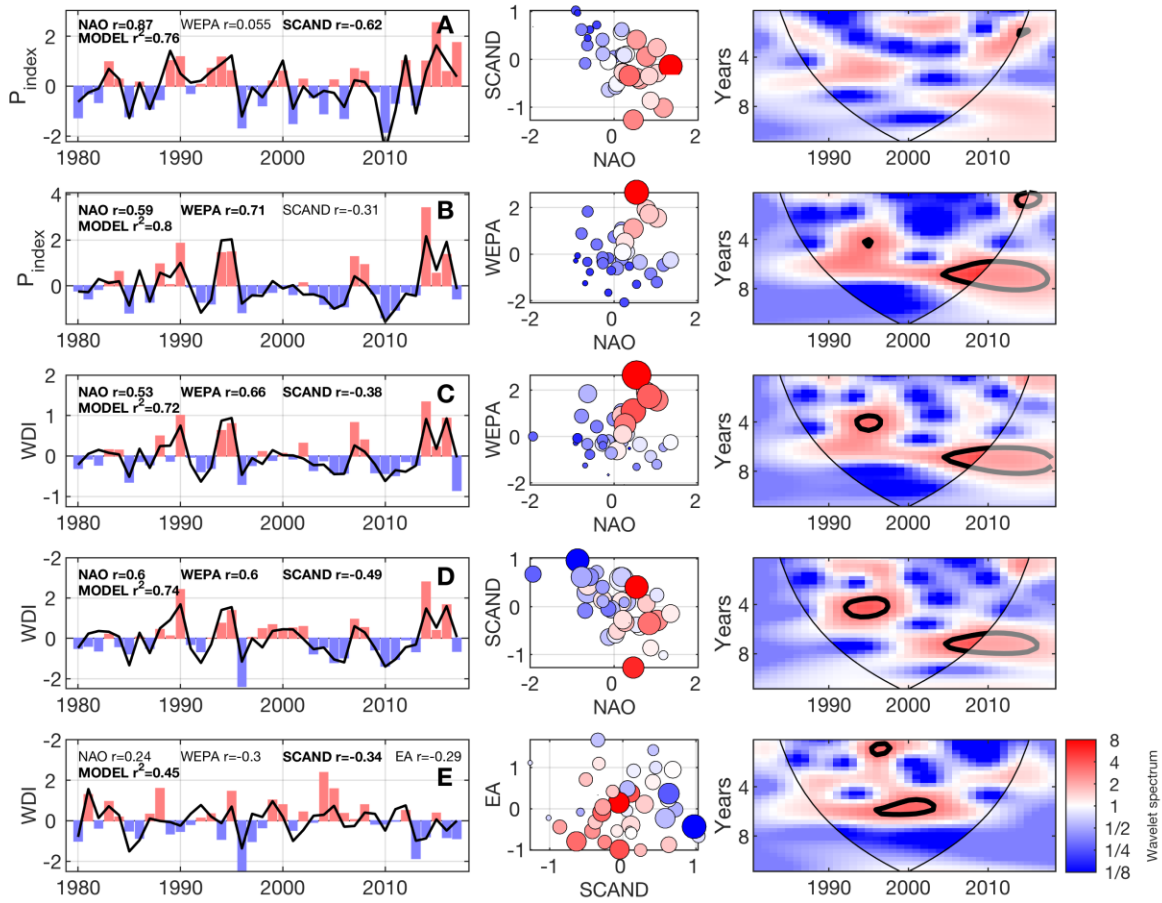388    +SCAND).

**Figure 7.** Temporal variability of standardized winter-averaged wave power ($P_{index}$; uni-directional regions) and wave direction (WDI; bi-directional regions) for case study sites from each of the 4 major classified regions are shown. Locations of sites A-E are shown on Figure 6. Left panels show 1980-2017 wave power ($P_{index}$; top two panels A-B) and winter-averaged WDI timeseries (bottom three panels C-E) for each winter season as red/blue bars, for each site correlations (r) with winter-averaged NAO, WEPA and SCAND are shown (bold is significant at the 95% level). In addition, stepwise multiple linear regression (SMLR) model r-squared values are shown (bold is significant at the 95% level) and model prediction line is shown (bold black). Middle panels show winter-averaged $P_{index}$ (top two) and WDI values (bottom three) within a 2D parameter space of the leading explanatory variables from SMLR for each site. Color is $P_{index}$ or WDI (low/high = blue/red, white = zero), bubble size is standardized winter wave power. Right panel shows local wavelet spectrum normalized by the variance of associated power and wave direction index. In wavelet panels, the 5% significance level against red noise is contoured in bold black line and the cone of influence is delimited by the fine black line.

389

390

391　The atmospheric expression of modelled $P_{index}$ and WDI values from case study sites for each
392　classified region (1980–2017) are explored in Figure 8 by taking the highest and lowest 5 years
393　for each $P_{index}$ (the same methodology as Figure 2). The highest five $P_{index}$ years (P+) at North
394　West and South West example sites (site A and site B) reflect the atmospheric signature NAO+
395　and WEPA+, respectively (Figure 2). In both sites (in particular site B), the influence of the
396　positive and negative SCAND patterns can be seen in both surface winds and the NAJ anomaly.
397　The P+ anomaly seen in the North West group case (site A) is expressed as an increase in
398　northwesterly surface winds above 55°N and a northward shift of the NAJ, while in the South
399　West group case (site B) P+ corresponds to a clockwise rotation of the NAJ with a striking
400　southward dip below 50°N over UK&I and NW Europe; this NAJ southerly shift is somewhat
401　characteristic of WEPA+ and SCAND-. Certainly, the most significant difference in P+ between
402　the North West and South West group cases is the increase in westerly surface winds below 53°N
403　(southern Ireland) for the latter when compared to a NAO+ (P+ site A) scenario. This observed
404　relationship between the NAJ and NAO is unsurprising and as year-to-year variability in the
405　NAO is known to describe the state of the Atlantic jet stream which is directly related to near-
406　surface winds across North America, Europe, and other regions around the Atlantic Basin (Scaife
407　et al. 2014)For the bi-directional South group (site C), the WDI+ expression is strongly reflected
408　in WEPA+ with increased westerly surface winds over the southern half of the UK&I. The WDI-
409　expression is one of increased southeasterly anomalies in surface winds throughout the English
410　Channel and North Sea and a dramatic reduction in westerly winds in the North Atlantic, limiting
411　southwesterly swell in this region; this is associated with an Atlantic shift of the NAJ to the north
412　(>65°N) or south (<45°N) away from the western approaches and reflects patterns of SCAND+
413　and NAO-. The WDI+ atmospheric expression from the East group (site E) shows a very strong
414　latitudinal shift of the NAJ below 50°N represented by a reduction in NAJ windspeeds of ~5 ms$^{-1}$
415　throughout the north and increase to the south. A strong northeast surface wind anomaly (> 2 ms$^{-1}$
416　) above 50°N throughout the North Sea and NE Atlantic represents a condition that may be
417　representative of increased northerly swell wave propagation into the North Sea. This pattern is
418　not clearly reflected in NAO, WEPA or SCAND, but can be partially reflected in the EA- pattern
419　(Figure 2). The signature of WDI- in the East group is even less clear reflecting the complexity
420　of the wave climate and highlight issues/limitations of trying to use climate indices to predict
421　directional wave climate in this region (East).

422　**6. Discussion and conclusions**

423　　　This study has shown there exists strong and significant connections between leading
424　climate indices in the North Atlantic and winter-averaged wave power in inshore regions, both in
425　exposed and (semi)- sheltered coastlines. For the first time, we have demonstrated the full extent
426　of directionally bimodal inshore wave climates around the coast of the UK&I, as well as the
427　significant role climate indices play in explaining their inter-annual variability over four decades.
428　It is well established that climate indices like ENSO in the Pacific and AO/NAO in the Atlantic
429　are leading modes of atmospheric variability and strongly affect winter wave energy (Dodet et
430　al., 2010; Bromirski et al., 2013; Castelle et al., 2017), and recent studies have also shown how
431　extreme phases can lead to large-scale coastal erosion and shoreline change (Masselink et al.,
432　2016; Barnard et al., 2017; Dodet et al., 2018). But, there is now a growing base of evidence
433　highlighting the role leading modes of climate variability also have in controlling wave direction
434　and associated longshore sediment re-distribution and shoreline rotation at the coast (e.g., Silva
435　et al., 2012; Splinter et al., 2014; Goodwin et al., 2016; Wiggins et al., 2019b). In extreme cases,
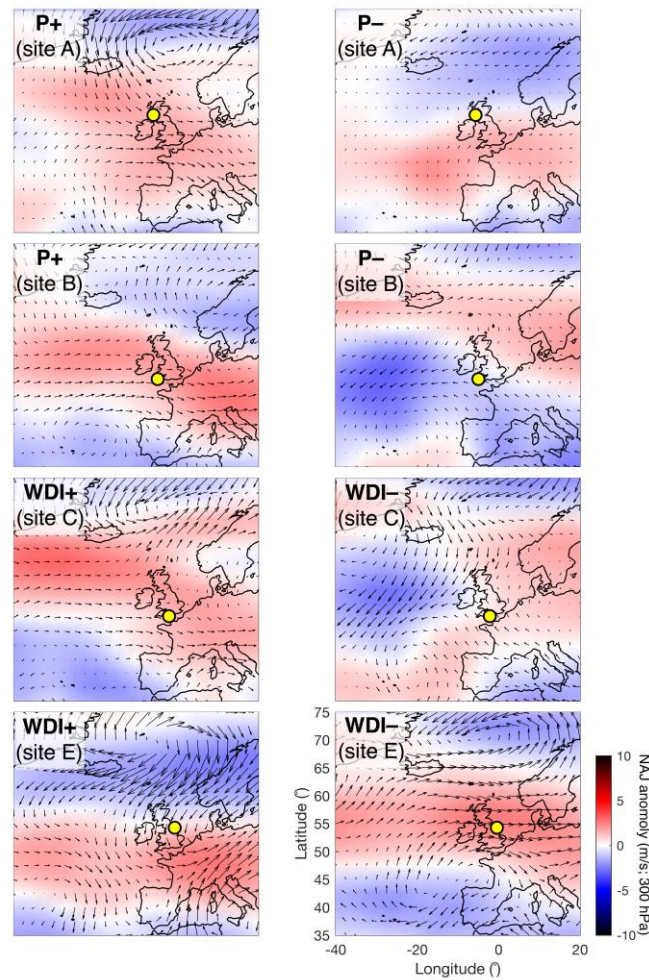
**Figure 8.** Atmospheric expressions of the directional wave power indices ($P_{index}$ and WDI) for example sites (yellow circles; A, B, C, and E) in each response group (North West, South West, South and East; top to bottom). Methodology and symbology as per Figure 2.

**Table 2.** Stepwise multiple linear regression models for winter-mean wave power (sites A and B) and WDI (sites C, D and E) as a function of combined climate indices. Coefficients are standardized weightings of significant variables used in the model.

| Site | Index | Weight | RMSE | $r^2$ | p-value |
|------|-------|--------|------|-------|---------|
| A (NorthWest) | NAO | 1.29 | 0.50 | 0.76 | $2 \times 10^{-12}$ |
| B (SouthWest) | NAO*WEPA | 0.32 | 0.46 | 0.8 | $4 \times 10^{-12}$ |
| C (South) | NAO*WEPA<br>SCAND | 0.33<br>-0.49 | 0.56 | 0.72 | $9 \times 10^{-9}$ |
| D (South) | NAO<br>WEPA<br>SCAND | 0.47<br>0.59<br>-0.68 | 0.54 | 0.73 | $2 \times 10^{-9}$ |
| E (East) | NAO* SCAND<br>WEPA* SCAND<br>SCAND*EA | 0.74<br>-1.18<br>1.47 | 0.82 | 0.45 | $25 \times 10^{-3}$ |

437  as shown by Wiggins et al. (2019a) when studying the impacts of the extreme storm wave events
438  of the 2013/14 winter in Northwest Europe, resultant embayment rotation in semi-sheltered
439  regions can lead to extreme coastal vulnerability and infrastructural failure.

440     These relationships between climate variability and inshore directional wave forcing are
441  critical for our understanding of multi-annual and multi-decadal coastal dynamics. The analysis
442  of 37 years of hindcast wave data from 63 inshore nodes around the entire coast of UK&I has
443  shown that 73% of studied sites have directionally bimodal wave climates (where secondary
444  modes are > 5% of primary mode peak prominence), with all sites within the English Channel
445  and North Sea regions found to be directionally bimodal. Of specific relevance to coastal
446  dynamics, primary and secondary modes within the English Channel and the southern North Sea
447  coasts are opposing with respect to the coastal normal and have the greatest potential to influence
448  coastal morphodynamics due to the importance of the directional balance of alongshore wave
449  power. This is evidenced by Wiggins et al. (2019) through the examination of a decade of beach
450  observations and embayment rotation along the south coast of England. Importantly, the analysis
451  of these wave directional modes as a function of leading climatic indices found that
452  combinations of the NAO, WEPA, SCAND and EA significantly explained the directional
453  variability in winter-averaged directional wave power throughout all coasts and modal directions
454  within the UK&I.

455     The seasonal variability of directional winter wave power throughout the UK&I also
456  demonstrated clear regional coherence. Cluster analysis of all coastal nodes driven by winter-
457  averaged directional wave correlations with NAO, WEPA, SCAND, AO and EA for the period
458  1980–2017 identified four key regions that had distinct responses to atmospheric variability. The
459  classes were strongly defined by wave exposure, coastal orientation and latitude; and the regional
460  classes were closely related to the impact that sea surface and NAJ wind expressions of related
461  indices could have on directional waves. Empirical multiple linear regression for regional
462  examples from each class demonstrated significant skill ($r^2 = 0.5$–$0.8$) for both uni- and bi-
463  directional sites, where skill in bi-directional sites was significantly improved through the
464  combination of multiple indices when variability of contrasting directional modes was explained
465  by different indices. Similar observations were made by Woollings et al. (2010) who had some
466  success in explaining the location and strength of the NAJ with a statistical mixture model
467  defined by the NAO and the EA (similar to WEPA).

468     The relation between large scale seasonal atmospheric behavior and wave directionality
469  along both exposed and more sheltered coasts that are dominated by longshore sediment
470  transport processes is important to enable development of skillful long range forecasting of
471  coastal dynamics. A similar approach has seen some success in seasonal forecasts of precipitation
472  in the UK (Baker et al., 2018). These relationships can also facilitate the extension of our
473  understanding of past (historic) coastal behavior, due to the fact atmospheric sea level pressure
474  (and proxy) records (e.g. Luterbacher et a., 1999; Camus et al., 2014) and modelled wave re-
475  analysis' (e.g. Santo et al., 2015), whist containing inherent uncertainties, are much longer than
476  those of sea surface waves or coastal morphological observations (<40 years; e.g., Turner et al.,
477  2016). The extent of variability and periodicity of each of the leading atmospheric indices
478  provides insights into coastal geomorphological response of beaches past and present (e.g.,
479  Castelle et al., 2018). As shown recently by Dodet et al. (2019), coastal (beach/dune) response to
480  the disturbance of extreme winters can be multi-annual and the rate and extent of beach recovery

481    is critically related to subsequent winter wave power and directionality. Therefore, an improved
482    understanding of multi-annual to decadal variability in wave conditions and its potential
483    prediction will be fundamental knowledge for future coastal management. In this respect, the
484    recently launched (October 2018) French-Chinese satellite CFOSAT designed to measure
485    simultaneously directional wave spectra and winds with innovative radar scatterometer onboard
486    (Hauser et al., 2019), will complement the spaceborne wave spectra measurements from
487    Synthetic Aperture Radar (Alpers et al., 1981), and allow an improved characterization of wave
488    spectral variability at the global scale.

489        6.1 Season-ahead forecasting

490        In this context, it is useful to examine the current skill of 'season ahead' forecasts of
491    winter-mean climate indices for explaining directional waves in the UK&I. Until recently, long-
492    range forecast systems showed only modest skill in 'season ahead' predictions of Atlantic winter
493    climate and the NAO, partially due to the lack of response of extratropical atmospheric
494    circulation to long-term predictive variability of the ocean (Smith et al., 2012). However, Scaife
495    et al. (2014) recently demonstrated significant skill (r = 0.6) in predicting the NAO when
496    initialized a month before the onset of winter and argued that greater ensemble sizes would kead
497    to greater skill (Scaife et al., 2014). One would expect from results presented in this study that
498    wave nodes in the North West group, that were highly correlated with the NAO, would be the
499    most forecastable. Indeed, this is borne out in Figure 9, where all uni-directional nodes between
500    southwest Ireland and north Scotland are significantly correlated (at 95% level) with forecast
501    NAO (1980–2016) where r= 0.37–0.52. This relationship disappears for the South West group,
502    where variability is more strongly linked to WEPA. Correlation scores for the bi-directional
503    groups South and East showed significant inverse correlations (at 95% level) with secondary
504    mode easterly waves at six sites along the English Channel coast, specifically those sites with a
505    southeasterly orientation. At the 90% level, the easterly wave component of wave climate
506    throughout English Channel and southern North Sea is significantly negatively correlated with
507    forecast NAO. For sites in the South and East groups, this skill does not translate into
508    predictability of WDI due to the strong influence of WEPA explaining the primary southwesterly
509    directional waves. To the authors' knowledge, these findings are the first demonstration of
510    skillful 'season ahead' forecasts for inshore directional winter wave climate and provide new
511    evidence that medium term forecasts of coastal hazard are currently achievable for selected
512    regions of the UK&I, and further advances in forecast skill may open the possibility for highly
513    valuable national scale coastal vulnerability assessments.

514        As noted by Scaife et al. (2014), much of the forecast skill of the atmospheric model is
515    derived from the ability to predict the NAO and this is highlighted by the lack of model skill in
516    regions where NAO influence is weak. It is therefore unsurprising that indices explaining
517    secondary modes of variability like WEPA are currently not well predicted (r = 0.13; p= 0.353).
518    An examination of the skill map for predicting DJFM Mean Sea Level Pressure (MSLP, Figure
519    10) confirms that, on average, DePreSys3 shows little MSLP skill over UK&I (located in the
520    region of high uncertainty due to the NAJ variability). Instead, significant skill is found to the
521    South (over the Azores/Southern Europe) and to the North (north of Iceland and over
522    Scandinavia). While this is a limitation for the UK&I and indices like WEPA, this does suggest
523    that the implementation of the approach used in this study in regions of greater atmospheric
524    model skill may yield stronger results. Encouragingly, recent studies have highlighted the
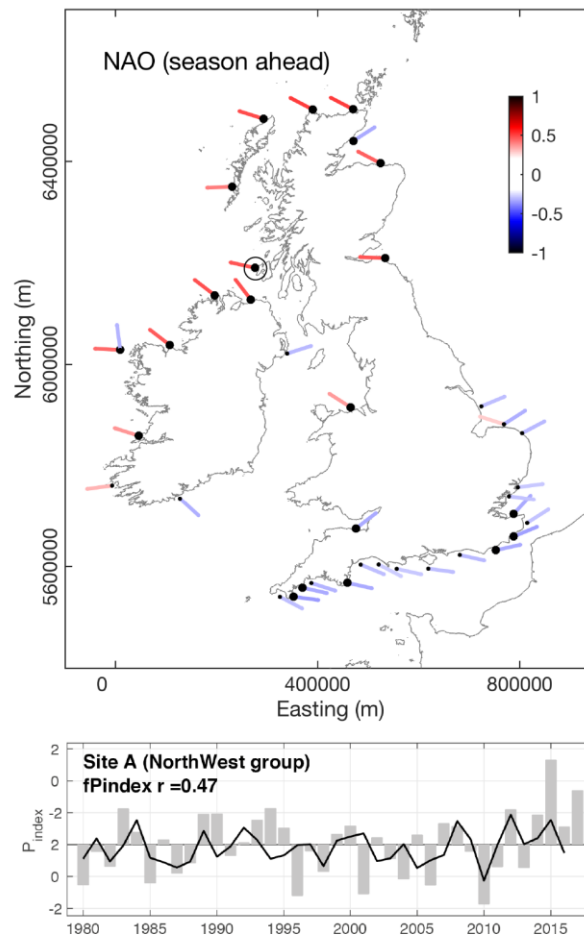
**Figure 9.** NAO 'season ahead' forecast: (upper) relationship between season-ahead forecast winter NAO and directional winter-averaged wave power (local wave directional window of +/- 20˚ for each node ) for 63 wave nodes around the coast of the UK&I (1980–2016). Colors are correlation coefficients (r), only results where P< 0.1 are shown, larger black dots represent P< 0.05. (lower) Winter $P_{index}$ timeseries for site A (NorthWest group) showing (black line) modelled $P_{index}$ values using forecast NAO from DePrySys 3 model. Correlation coefficient is significant at 95% level.

525
526 potential for future improvements in seasonal (Athanasiadis et al., 2016) and decadal (Smith et
527 al., 2019) forecast skill through increased ensemble sizes, citing the 'signal to noise paradox',
528 which identifies that climate models (particularly for the Atlantic) are better able to predict their
529 observed counterparts than their weak signal-to-noise ratios may suggest, meaning there may be
530 much more potential predictability of indices like the NAO with larger ensemble sizes (Scaife
531 and Smith, 2018). In combination with the indication that the seasonal and decadal climate may
532 be more predictable than previously thought, the strong relationships uncovered in this study
533 between inshore winter waves and atmospheric indices suggests that the potential for skillful
534 long-term wave climate forecasts may be realized in the near future. This would better enable
535 decision-makers to effectively adapt to the impact of long-term climate variability and extreme
536 events (Smith et al., 2019).

537    Within the global coastal science community there is an ever-increasing focus on
538 developing skillful long-term predictions of coastal evolution due to climate change (through
539 increased sea-level rise and changes in storminess; e.g., Montano et al., 2020). As part of this
540 challenge, it will be critical to account for climate variability and put observed coastal change
541 over the past 20 years into this context. As elucidated through climate indices like the NAO,
542 these indices can reflect natural variability in the ocean and atmosphere on inter-annual and
543 multi-decadal scales (e.g., Scaife et al., 2014; Wang et al., 2016; McCarthy et al., 2018). Deser et
544 al. (2017) suggested that internal variability of the NAO imparts substantial uncertainty in future
545 changes in regional climate even out to decades ahead. This is likely overestimated due to signal
546 to noise errors in predictions of the NAO (Eade et al 2014) but still needs to be accounted for in
547 climate projections and predictions of directional wave climate in order to aid coastal managers
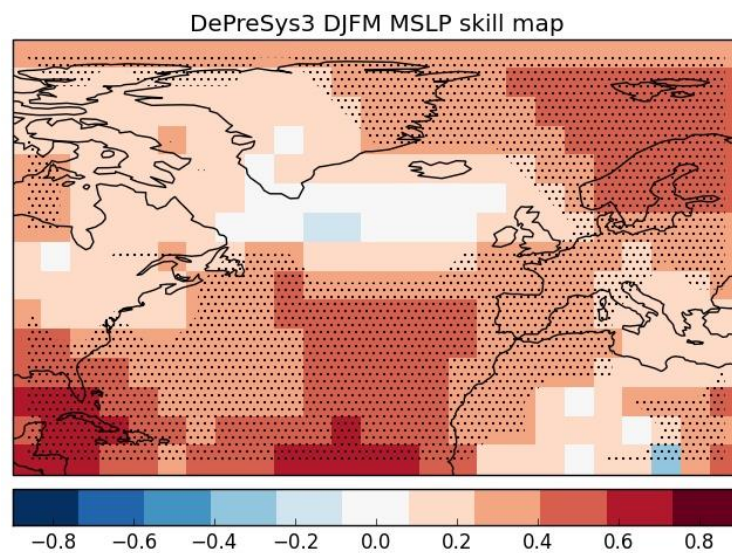548 to prepare and adapt to ongoing climate variability and change.



**Figure 10.** Spatial distribution of skill (correlation) for UK Met Office Decadal Climate Predication System 3 (DePreSys3), predicting the season ahead winter (DJFM) mean sea level pressure. Stippled regions are significant at the 5% level according to a Student's t-test.

549

## Acknowledgements

560 this study are publicly available for the period 1980–2017 (National Oceanic and Atmospheric
561 Administration (NOAA) Climate Prediction Center; www.cpc.ncep.noaa.gov). The Western
562 Europe Pressure Anomaly (WEPA) climate index (1943-2018) developed by Castelle et al.
563 (2017) is publicly available online via the University of Plymouth PEARL open access research
564 repository (http://hdl.handle.net/10026.1/15509). Season-ahead retrospective forecasts
565 (hindcasts) of the winter-averaged December-March (DJFM) NAO and WEPA are not publicly
566 available due to commercial restrictions, but can be sourced from the Met Office
567 (enquiries@metoffice.gov.uk)  for specific research purposes.

## References

569       Alpers, W.R., Ross, D.B., Rufenach, C.L., 1981. On the detectability of ocean surface
570 waves by real and synthetic aperture radar. Journal of Geophysical Research: Oceans 86, 6481–
571 6498. https://doi.org/10.1029/JC086iC07p06481

572       Antolínez, J. A. A., Murray, A. B., Méndez, F. J., Moore, L. J., Farley, G., and Wood, J.
573 (2018). Downscaling changing coastlines in a changing climate: The hybrid approach. Journal of
574 Geophysical Research: Earth Surface, 123(2), 229-251

575       Athanasiadis, P., Bellucci, A., Scaife, A. A., Hermanson, L., Materia, S., Sanna, A.,
576 Borrelli, A., MacLachlan, C. and Gualdi, S. (2016). A multi-system view of wintertime NAO
577 seasonal predictions. Journal of  Climate, 30, 1461–1475. doi:10.1175/JCLI-D-16-0153.1

578       Baker, L. H., Shaffrey, L. C., Sutton, R. T., Weisheimer, A., & Scaife, A. A. (2018). An
579 intercomparison of skill and overconfidence/underconfidence of the wintertime North Atlantic
580 Oscillation in multimodel seasonal forecasts. Geophysical Research Letters, 45, 7808–7817.
581 https://doi.org/10.1029/2018GL078838

582       Barbosa, S., Silva, M. E., and Fernandes, M. J. (2006). Wavelet analysis of the Lisbon
583 and Gibraltar North Atlantic Oscillation winter indices. International Journal of Climatology,
584 26(5), 581–593.

585       Barnard, P. L., A. D. Short, M. D. Harley, K. D. Splinter, S. Vitousek, I. L. Turner, J.
586 Allan, et al. (2015). Coastal Vulnerability across the Pacific Dominated by El Niño/Southern
587 Oscillation, Nature Geoscience 8: 801–807.

588       Barnston, A. G., Livezey, R. E., (1987) Classification, seasonality and persistence of low-
589 frequency atmospheric circulation patterns. Monthly Weather Review, 115, 1083–1126.

590       Bergillos, R.J., Ortega-Sánchez, M., Masselink, G., Losada, M.A. (2016). Morpho-
591 sedimentary dynamics of a micro-tidal mixed sand and gravel beach, Playa Granada, southern
592 Spain. Marine Geology. 379, 28–38.

593       Burvingt, O., Masselink, G., Scott, T., Davidson, M., Russell, P. (2018). Climate forcing
594 of regionally-coherent extreme storm impact and recovery on embayed beaches. Marine Geology
595 401, 112–128.

596       Bromirski, P. D., Cayan, D. R., Helly, J., and Wittmann, P. (2013).Wave power variability

597    and trends across the North Pacific. Journal of Geophysical Research: Oceans, 118, 6329–6348.
598    https://doi.org/10.1002/2013JC009189

599    Buhler O. and T.E. Jacobson (2001). Wave-driven currents and vortex dynamics on
600    barred beaches. J. Fluid Mech., 449, 313-319.

601    Camus, P., Menéndez, M., Méndez, F. J., Izaguirre, C., Espejo, A., Cánovas, V., ... and
602    Medina, R. (2014). A weather-type statistical downscaling framework for ocean wave climate.
603    Journal of Geophysical Research: Oceans, 119(11), 7389-7405.

604    Castelle, B., Coco, G. (2012). The morphodynamics of rip channels on embayed beaches.
605    Continental Shelf Research, 43, 10–23, doi: 10.1016/j.csr.2012.04.010.

606    Castelle, B., Marieu, V., Bujan, S., Ferreira, S., Parisot, J. P., Capo, S., et al. (2014).
607    Equilibrium shoreline modelling of a high-energy meso-macrotidal multiple-barred beach.
608    Marine Geology, 347, 85–94.

609    Castelle, B., Dodet, G., Dodet, G., Scott, T. (2017). A new climate index controlling
610    winter wave activity along the Atlantic coast of Europe: the West Europe Pressure Anomaly.
611    Geophysical Research Letters,  44, 1384–1392.

612    Castelle, B., Dodet, G., Masselink, G., and Scott, T. (2018). Increased winter-mean wave
613    height, variability, and periodicity in the Northeast Atlantic over 1949-2017, Geophysical
614    Research Letters, 45(8), 3586-3596.

615    Cazenave, A., Dieng, H.-B., Meyssignac, B., von Schuckmann, K., Decharme, B.,
616    Berthier, E. (2014). The rate of sea-level rise. Nature Climate Change, 4, 358-361,
617    doi:10.1038/nclimate2159.

618    Colman, A. W., Palin, E. J., Sanderson, M. G., Harrison, R. T., & Leggett, I. M. (2011).
619    The potential for seasonal forecasting of winter wave heights in the northern North Sea. Weather
620    and Forecasting, 26( 6), 1067– 1074.

621    Deser, C., Hurrell, J. W. and Phillips, A. S. (2017). The role of the North Atlantic
622    Oscillation in European climate projections. Climate Dynamics, 49 (9), 3141—3157.

623    Dobrynin M, T. Kleine, A. Düsterhus and J. Baehr (2019). Skilful Seasonal Prediction of
624    Ocean Surface Waves in the Atlantic Ocean. Geophys. Res. Lett., 46, 1731– 1739.

625    Dodet, G., Bertin, X., Taborda, R. (2010). Wave climate variability in the North-East
626    Atlantic Ocean over the last six decades. Ocean Modelling 31, 120–131.
627    https://doi.org/10.1016/j.ocemod.2009.10.010

628    Dodet, G., Castelle, B., Masselink, G., Scott, T., Davidson, M., Floc'h, F., Jackson, D.,
629    and Suanez, S. (2018). Beach recovery from extreme storm activity during the 2013/14 winter
630    along the Atlantic coast of Europe. Earth Surface Processes and Landforms, 44 (1) 393-401.

631    Dunstone, N., Smith, D., Scaife, A. A., Hermanson, L., Eade, R., Robinson, N., et al.

632    (2016). Skilful predictions of the winter North Atlantic Oscillation one year ahead. Nature
633    Geoscience, 9, 809–814.

634        Eade R., D. Smith, A.A. Scaife and E. Wallace, 2014. Do seasonal to decadal climate
635    predictions underestimate the predictability of the real world? Geophys. Res. Lett., 41, 5620–
636    5628.

637        Harley, M.D., Turner, I.L., Short, A.D., Ranasinghe, R. (2011). A reevaluation of coastal
638    embayment rotation: the dominance of cross-shore versus alongshore sediment transport
639    processes, Collaroy-Narrabeen Beach, southeast Australia. Journal of Geophysical Research:
640    Earth Surface, 116, 1–16.

641        Harley, M.D., I.L. Turner, M.A. Kinsela, J.H. Middleton, P.J. Mumford, K.D. Splinter,
642    M.S. Phillips, J.A. Simmons, D.J. Hanslow, and A.D. Short. (2017). Extreme coastal erosion
643    enhanced by anomalous extratropical storm wave direction. Nature Scientific Reports 7:6033.

644        CFOSAT: A New Mission in Orbit to Observe Simultaneously Wind and Waves at the
645    Ocean Surface, 2019. . Space Research Today 206, 15–21.
646    https://doi.org/10.1016/j.srt.2019.11.012

647        Hurrell, J. W. (1995), Decadal Trends in the North Atlantic Oscillation: Regional
648    Temperatures and Precipitation, Science, 269(5224), 676–679

649        Goodwin, I. D., Mortlock, T. R. and Browning, S. (2016). Tropical and extratropical-
650    origin storm wave types and their influence on the East Australian longshore sand transport
651    system under a changing climate. Journal of Geophysical Research: Ocean. 121, 4833–4853.

652        Grinsted, A., Moore, J. C., Jevrejeva, S. (2004). Application of the cross wavelet
653    transform and wavelet coherence to geophysical time series. Nonlinear Processes in Geophysics,
654    11, 561566.

655        Itoh, H. (2008). Reconsideration of the true versus apparent Arctic Oscillation. Journal of
656    Climatology 21(10): 2047–2062.

657        Kalnay, E., and Coauthors, (1996). The NCEP/NCAR 40-year Reanalysis Project.
658    Bulletin of the American Meteorological Society, 77, 437-471.

659        Kim, H. M., Webster, P. and Curry, J. (2012). Seasonal prediction skill of ECMWF
660    System 4 and NCEP CFSv2 retrospective forecast for the Northern Hemisphere winter. Climate
661    Dynamics 23, 2957-2973.

662        Klein, A.H.D.F., Filho, L.B., Schumacher, D.H. (2002). Short-term beach rotation
663    processes in distinct headland bay beach systems. Journal of Coastal Research, 18, 442–458.

664        Le Cozannet, G., Oliveros, C., Castelle, B., Garcin, M., Idier, D., Pedreros, R., Rohmer, J.
665    (2016). Uncertainties in sandy shorelines evolution under the Bruun rule assumption. Frontiers
666    Marine Sciences, 3, doi:0.3389/fmars.2016.00049.

667    Ludka, B.C., Guza, R.T., O'Reilly, W.C. et al. (2019). Sixteen years of bathymetry and
668    waves at San Diego beaches. Scientific Data, 6, 161, doi:10.1038/s41597-019-0167-6.

669    Luterbacher, J., Schmutz, C., Gyalistras, D., Xoplaki, E., Wanner, H. (1999).
670    Reconstruction of monthly NAO and EU indices back to AD 1675. Geophysical Research Letters
671    26, 2745–2748. https://doi.org/10.1029/1999GL900576.

672    Luijendijk, A., Hagenaars, G., Ranasinghe, R., Baart, F., Donchyts, G., Aarninkhof, S.
673    (2018). The State of the World's Beaches. Scientific Reports, 8(1), doi:10.1038/s41598-018-
674    24630-6.

675    Martinez-Asensio. A., Tsimplis, M. N., Marcos, M., Feng, X., Gomis, D., Jorda, G. and
676    Josey, S. A. (2016). Response of the North Atlantic wave climate to atmospheric modes of
677    variability International Journal of Climatology, 36 1210–25.

678    Masselink, G., Castelle, B., Scott, T., Dodet, G., Suanez, S., Jackson, D., Floc'h, F.
679    (2016). Extreme wave activity during 2013/2014 winter and morphological impacts along the
680    Atlantic coast of Europe. Geophysical Research Letters 43: 2135–2143.

681    McCarthy, G. D., Joyce, T. M. M., and Josey, S. A. (2018). Gulf Stream variability in the
682    context of quasi-decadal and multidecadal Atlantic climate variability. Geophysical Research
683    Letters, 45, 11,257–11,264. https://doi.org/10.1029/2018GL079336

684    Mentaschi, L., Vousdoukas, M.I., Pekel, J.P., Voukouvalas, E., and Feyen, L. (2018).
685    Global long-term observations of coastal erosion and accretion. Scientific Report, 8: 12876,
686    doi:10.1038/s41598-018-30904-w.

687    Mitchell, J. A., Bett, P. E., Hanlon, H. M., Saulter, A. (2017). Investigating the impact of
688    climate change on the UK wave power climate. Meteorologische Zeitschrift.

689    Montaño, J., Coco, G., Alvarez, J. A., Beuzen, T., Bryan, K., Cagigal, L., Castelle, B.,
690    Davidson, M., Goldstein, E., Ibaceta, R., Idier, D., Ludka, B., Masoud-Ansari, S., Méndez, F.,
691    Murray, A. B., Plant, N., Ratliff, K., Robinet, A., Rueda Z. A., and Vos, K. (2020). Blind testing
692    of shoreline evolution models. Scientific Reports. 10. 10.1038/s41598-020-59018-y.

693    Mortlock, T.R., Goodwin, I.D. (2016). Impacts of enhanced central pacific ENSO on
694    wave climate and headland-bay beach morphology. Continental Shelf Research, 120, 14–25.

695    Poli, P., Hersbach, H., Dee, D. P., Berrisford, P., Simmons, A. J., Vitart, F., et al. (2016).
696    Era-20C: An atmospheric reanalysis of the twentieth century. Journal of Climate, 29(11), 4083–
697    4097. https://doi.org/10.1175/JCLI-D-15-0556.1

698    Ruiz de Alegria-Arzaburu, A., Masselink, G. (2010). Storm response and beach rotation
699    on a gravel beach, Slapton Sands, U.K. Marine Geology. 278, 77–99.

700    Santo, H., Taylor, P. H., Woollings, T., Poulson, S. (2015). Decadal wave power
701    variability in the North-East Atlantic and North Sea. Geophysical Research Letters 42, 4956-
702    4963. https://doi.org/10.1002/2015GL064488.

703 Saulter, A. (2015). Assessment of WAM Cycle-4 based source terms for the Met Office
704 global-regional wave modelling system. Forecasting Research Technical Report 598, Met Office,
705 Exeter, UK.

706 Scaife A.A., T. Spangehl, D. Fereday, U. Cubasch, U. Langematz, H. Akiyoshi, S. Bekki,
707 P. Braesicke, N. Butchart, M. Chipperfield, A. Gettelman, S. Hardiman, M. Michou, E. Rozanov
708 and T.G. Shepherd 2012. Climate Change and Stratosphere-Troposphere Interaction. Clim. Dyn.,
709 38, 2089-2097.

710 Scaife, A. A. et al. (2014). Skillful long-range prediction of European and North
711 American winters. Geophysical Research Letters. 41, 2514–2519.

712 Scaife, A. A. and D. Smith, (2018). A signal-to-noise paradox in climate science. NPJ:
713 Climate and Atmospheric Science, 1, http://dx.doi.org/10.1038/s41612-018-0038-4.

714 Scott, T., Masselink, G., Hare, T.O., Saulter, A., Poate, T., Russell, P., Davidson, M.,
715 Conley, D. (2016). The extreme 2013/2014 winter storms: beach recovery along the southwest
716 coast of England. Mar. Geol. 382, 224–241.

717 Short, A.D., Masselink, G. (1999). Handbook of beach and shoreface morphodynamics.
718 Embayed and Structurally Controlled Beaches. John Wiley.

719 Silva, A.N., Taborda, R., Bertin, X., Dodet, G. (2012). Seasonal to Decadal Variability of
720 Longshore Sand Transport at the Northwest Coast of Portugal. Journal of Waterway, Port,
721 Coastal, and Ocean Engineering 138, 464–472. https://doi.org/10.1061/(ASCE)WW.1943-
722 5460.0000152

723 Splinter, K. D., Davidson, M. A., Golshani, A., and Tomlinson, R. (2012). Climate
724 Controls on Longshore Sediment Transport. Continental Shelf Research 48, 146–156.

725 Smith, D., Scaife, A. A., and Kirtman, B. (2012). What is the current state of scientific
726 knowledge with regard to seasonal and decadal forecasting? Environmental Research Letters., 7,
727 015602.

728 Smith, D. M., Scaife, A. A., Eade, R. & Knight, J. R. (2016). Seasonal to decadal
729 prediction of the winter North Atlantic Oscillation: emerging capability and future prospects. Q.
730 J. R. Meteorol. Soc. 142, 611–617.

731 Smith, D. M., Eade, R., Scaife, A. A. et al. (2019). Robust skill of decadal climate
732 predictions. NPJ: Climate and Atmospheric Sciences, 2 (13).

733 Tolman, H.L. (2009). User manual and system documentation of WAVEWATCH IIITM
734 version 3.14. – NOAA/NWS/NCEP/ MMAB Technical Note 276, Environmental Modeling
735 Center, Marine Modeling and Analysis Branch.

736 Turner, I. L., Harley, M. D., Short, A. D., Simmons, J. A., Bracs, M. A., Phillips, M. S.,
737 Splinter, K. D. (2016). A multi-decade dataset of monthly beach profile surveys and inshore
738 wave forcing at Narrabeen, Australia, Scientific Data, vol. 3,

739   http://dx.doi.org/10.1038/sdata.2016.24

740   Vousdoukas, M.I., Mentaschi, L., Voukouvalas, E., Verlaan, M., Jevrejeva, S., Jackson,
741   L.P., Feyen, L. (2018). Global probabilistic projections of extreme sea levels show intensification
742   of coastal flood hazard. Nature Communications, 9: 2360, doi:10.1038/s41467-018-04692-w.

743   Wang, L., Ting, M., and Kushner, P. (2017). A robust empirical seasonal prediction of
744   winter NAO and surface climate. Scientific Reports, 7(1), 279. https://doi.org/10.1038/s41598-
745   017-00353-y

746   Ward, J. H. (1963). Hierarchical grouping to optimize an objective function, Journal of
747   the American Statistical Association, 58, 236-244.

748   Wiggins, M. A., Scott, T., Masselink, G., Russell, P., and McCarroll, R. (2019a). Coastal
749   embayment rotation: Response to extreme events and climate control, using full embayment
750   surveys. Geomorphology, 327, 385-403.

751   Wiggins, M., Scott, T., Masselink, G., Russell, P., Valiente, N.G. (2019b). Regionally-
752   Coherent Embayment Rotation: Behavioural Response to Bi-Directional Waves and Atmospheric
753   Forcing. Journal of Marine Science and Engineering. 2019, 7, 116.

754   Woollings T, Hannachi A, Hoskins B. (2010). Variability of the North Atlantic eddy-
755   driven jet stream. Q. J. R. Meteorol. Soc. 136(649): 856–868. https://doi.org/10.1002/qj.625.